Double Perovskite Single-Crystal Photoluminescence Quenching and Resurge

Ito, Bruno I.; Tekelenburg, Eelco K.; Blake, Graeme R.; Loi, Maria A.; Nogueira, Ana Flavia

Published in:
JOURNAL OF PHYSICAL CHEMISTRY LETTERS

DOI:
10.1021/acs.jpclett.1c03035

Publication date:
2021

THE JOURNAL OF PHYSICAL CHEMISTRY LETTERS
A JOURNAL OF THE AMERICAN CHEMICAL SOCIETY

pubs.acs.org/JPCL

Letter

Double Perovskite Single-Crystal Photoluminescence Quenching and Resurge: The Role of Cu Doping on its Photophysics and Crystal Structure

Bruno I. Ito, Eelco K. Tekelenburg, Graeme R. Blake, Maria A. Loi,* and Ana Flavia Nogueira*

Cite This: *J. Phys. Chem. Lett.* 2021, 12, 10444−10449

Read Online

ACCESS | Metrics & More | Article Recommendations | Supporting Information

ABSTRACT: $Cs_2AgBiBr_6$ is a potential lead-free double perovskite candidate for optoelectronic applications; however, its large and indirect band gap imposes limitations. Here, single crystals of $Cs_2AgBiBr_6$ are doped with Cu^{2+} cations to increase the absorption range from the visible region up to 0.5 eV in the near-infrared region. Inductively coupled plasma spectroscopy confirms the presence of 1.9% of copper in the $Cs_2AgBiBr_6$ structure. Structural and optical changes caused by Cu doping were studied by Raman spectroscopy combined with X-ray diffraction, heat capacity measurements, and low-temperature photoluminescence spectroscopy. Along with the 1.9 eV emission typical of the pristine $Cs_2AgBiBr_6$ single crystals, we report a novel low-energy emission at 0.9 eV related to deep defects. In the doped crystals, these peaks are quenched, and a new emission band at 1.3 eV is visible. This new emission band appears only above 120 K, showing that thermal energy is necessary to trigger the copper-related emission.

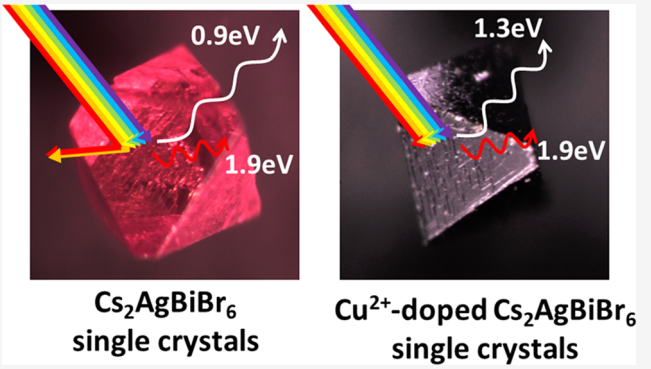

In recent years, metal halide perovskites (MHPs) have been positioned in the spotlight due to their impressive light-harvesting ability and power conversion performance in photovoltaic devices.[1−4] The most promising MHPs are Pb-based, presenting high absorption coefficients in the visible region, exceptional tolerance to defects, and low-cost and easy manufacturing processes.[5,6] On the other hand, Pb is toxic to the environment and human health, and the use of the water-soluble Pb^{2+} facilitates fast contamination.[7,8] Although there are several strategies to mitigate Pb toxicity, including encapsulation and recycling, current regulations may inhibit the commercialization of Pb-based perovskites.[9] Hence, replacing Pb with less toxic metals that preserve the remarkable photophysical properties would constitute a highly desirable advance of this field.

Lead-free double perovskites (LFDPs) have emerged as promising candidates because of the possibility of tuning their band gap and their higher stability in ambient conditions.[10] LFDPs are described by the general formula $A_2B'B''X_6$, where A and B′ are monovalent cations, B″ is a trivalent cation, and X is a halide. A well-studied prototypical example is the silver and bismuth-based perovskite $Cs_2AgBiBr_6$, which presents great ambient stability, has a relatively easy synthesis route, and consists of cheap and abundant elements.[11−13] Several studies have investigated the photophysical pathways after the excitation of $Cs_2AgBiBr_6$ single crystals and thin films. It has become clear that a fast picosecond relaxation occurs toward the conduction band edge, followed by up to a microsecond-long long-lived state.[14−16] The photoluminescence (PL) of $Cs_2AgBiBr_6$ typically shows a broad emission band with a large Stokes shift centered at 1.9 eV. While this PL band was initially attributed to recombination across the indirect band gap, recent studies have shown that the origin of this band is related to defects.[14,15,17,18] Hence, it has become clear that defects play an important role in this prototypical double perovskite. However, most studies have concentrated on the visible spectral range, showing only a part of the physical reality of this material. Besides the pronounced effect of defects, the large and indirect band gap of this composition hinders its potential as an efficient light-harvesting material. To overcome these drawbacks, several doping and alloying strategies have been reported. Slavney et al. introduced thallium (Tl) to the structure of $Cs_2AgBiBr_6$, demonstrating that Tl substitutes Bi^{3+} at low concentrations of Tl^{3+} and substitutes Ag^+ at high concentrations of Tl^+. The substitutions generated doping energy levels within the band gap, causing a shift of the indirect band gap from 1.95 to 1.4 eV and a shift of the direct band gap

Received: September 14, 2021
Accepted: October 20, 2021
Published: October 21, 2021

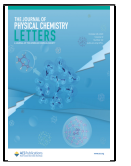

https://doi.org/10.1021/acs.jpclett.1c03035
J. Phys. Chem. Lett. 2021, 12, 10444−10449

from 2.21 to 1.57 eV.[19] Doping of $Cs_2AgBiBr_6$ with copper (Cu^+ and Cu^{2+}) ions was reported to replace Ag^+ and, in the case of divalent copper, create an additional Ag^+ vacancy defect to maintain charge neutrality.[20] It was shown that the Cu doping generated deep-level defect states at 1.3 eV from the band edge that changed the color of the crystals and enhanced the near-infrared response.[20] While this strategy was shown to effectively modify the absorption onset of $Cs_2AgBiBr_6$, very little is known on the impact of the Cu substitution on the structural properties and photophysics of this compound.

In this work, we dope $Cs_2AgBiBr_6$ single crystals with different Cu^{2+} concentrations and study their fundamental structural and optical properties in detail. At room temperature, we reveal that the copper doping shifts the Raman modes without altering the crystal structure. The pristine $Cs_2AgBiBr_6$ shows a PL peak at 1.9 eV together with a previously unreported peak at 0.9 eV, which we believe originates from deep defect levels. The Cu doping introduces additional defect levels that strongly modify the emission of the system, giving rise to a previously unreported emission band at around 1.3 eV. This new emission only appears above 120 K, showing that thermal energy is necessary to trigger this copper-related emission. We also provide evidence that the introduction of copper inhibits a structural phase transition at cryogenic temperatures. The understanding of this kind of doping is fundamental to have more insight into the promise of double perovskites for optoelectronic applications.

$Cs_2AgBiBr_6$ single crystals were synthesized using a modified hydrothermal method described in the literature.[16] The doping of $Cs_2AgBiBr_6$ single crystals with copper was achieved by the addition of copper(II) chloride ($CuCl_2$) to the reaction solution of the pristine (P) $Cs_2AgBiBr_6$, which will hereafter be referred to as D1−D5 for increasing Cu concentrations. Table S1 of the Supporting Information (SI) shows the concentrations of $CuCl_2$ used in the reaction solutions. The synthesized crystals are shown in Figure 1a, where the color gradually changes from red to black as the Cu concentration increases. To confirm the presence of copper in the crystals, we performed inductively coupled plasma optical emission spectroscopy (ICP-OES) on all the synthesized crystals, and the content of Cu (mol %) is presented in Table S1. We note that this Cu content includes both monovalent and divalent ions. The concentration of copper in the D1 and D2 crystals was below the detection limit of the ICP-OES equipment, but the presence of copper was confirmed for the D3, D4, and D5 crystals and reached 1.9% for D5. The structures of the crystals were analyzed by powder X-ray diffraction (PXRD), and the patterns are compared in Figure 1b. The PXRD pattern of sample P is consistent with the reported cubic structure.[16,21] The PXRD patterns of the crystals with different copper contents exhibit similar peak positions, suggesting that copper doping does not alter the crystal structure.

Raman spectra of the P and D1−D5 crystals were collected at room temperature to investigate changes of the vibrational modes by the introduction of copper (Figure 1c). $Cs_2AgBiBr_6$ presents three distinct Raman modes, which are related to (1) the motion of Cs atoms with the scissoring of Br atoms around Ag atoms ($T_{2g} \sim 76$ cm^{-1}), (2) the asymmetric stretching of Br atoms around Bi atoms in the octahedron ($E_{1g} \sim 135$ cm^{-1}), and (3) the symmetric stretching of Br atoms around Ag and Bi atoms in the octahedron ($A_{1g} \sim 179$ cm^{-1}).[17,22] Doping with copper shifts the E_{1g} and A_{1g} modes to lower energies and the T_{2g} mode to higher energies. Steele et al.

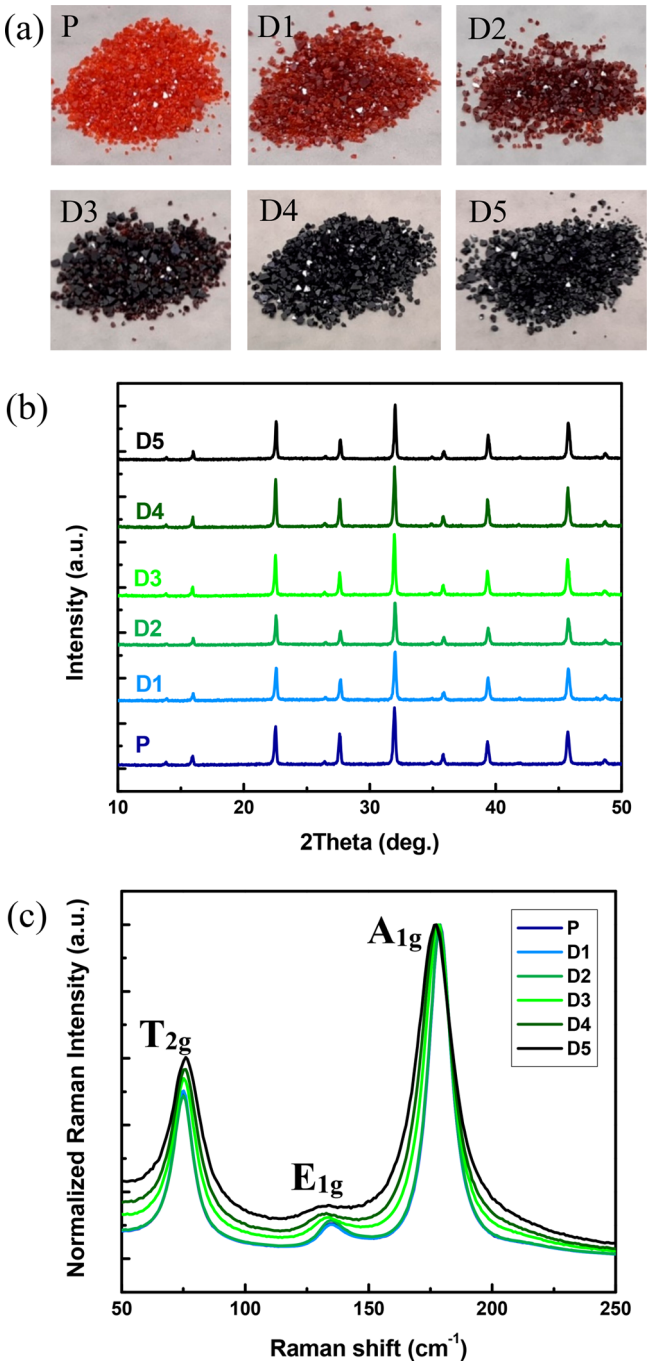

Figure 1. (a) Synthesized crystals identified as P (pristine) and D (doped) at different Cu concentrations with an approximately 400 μm size on average, (b) powder XRD data, and (c) normalized Raman data measured at room temperature for P and D1−D5 crystals.

proposed that the $Cs_2AgBiBr_6$ structure presents bonding distortions and strain because the calculated Ag−Br bond length of 3.11 Å differs significantly from the experimentally measured bond length of 2.828 Å.[22] On the other hand, the calculated bond length of Cu−Br is 2.69 Å. As copper is expected to substitute Ag^+ and create additional Ag^+ vacancies in the structure, the shifts of E_{1g} and A_{1g} might originate from a reduced bonding strain in the crystal structure.[20] Additionally, structural defects, such as Ag vacancies, caused by the introduction of copper could slightly shift the Cs scissoring. In conjunction with the shifts, the Raman peaks broadened

https://doi.org/10.1021/acs.jpclett.1c03035
J. Phys. Chem. Lett. 2021, 12, 10444−10449

with increasing copper concentration from approximately 11 to 18 cm^{-1}, suggesting increased disorder caused by copper-induced defects in the crystal.[23]

First, we will discuss the optical properties of the pristine material such that we obtain a benchmark for discussing the effect of copper doping. The diffuse reflectance Kubelka–Munk transformation and the PL of the pristine $Cs_2AgBiBr_6$ are shown in Figure 2a. The absorption onset at around 2.1 eV

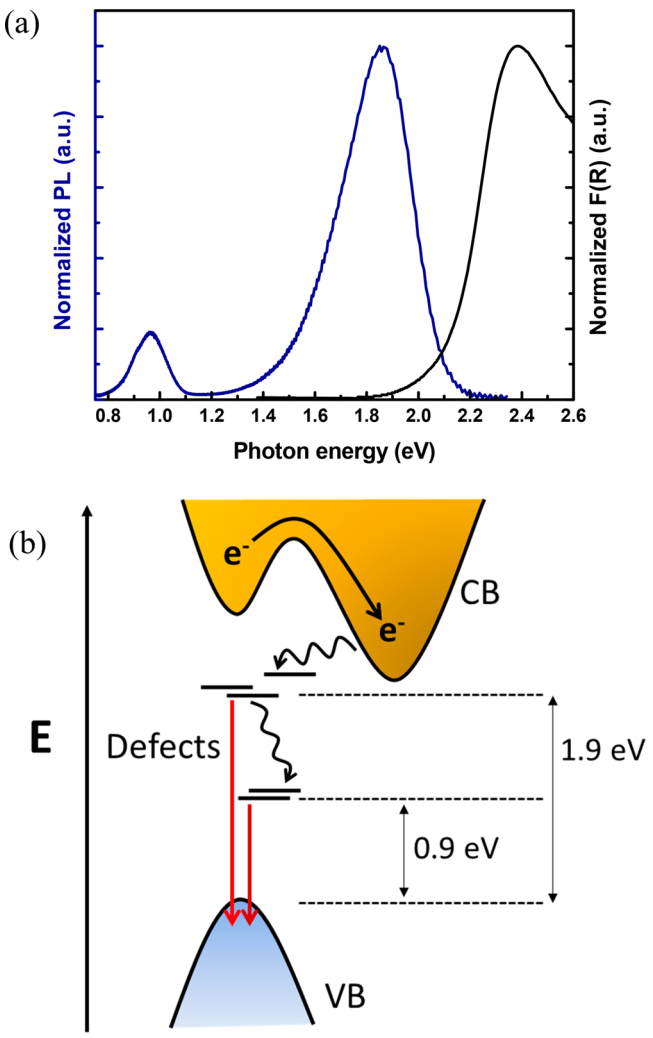

Figure 2. (a) Normalized photoluminescence and Kubelka–Munk-transformed diffuse reflectance spectra of pristine $Cs_2AgBiBr_6$ crystals and (b) schematic of the radiative recombination pathways associated with the defects in $Cs_2AgBiBr_6$.

is in line with recently reported values of the indirect band gap.[16,21,24] The PL of the pristine $Cs_2AgBiBr_6$ at room temperature is dominated by a broad PL peak centered around 1.9 eV, a commonly reported feature in this material.[16,24] There is a growing consensus that this peak originates from defect levels in the band gap as opposed to IT earlier attribution to recombination across the indirect band gap.[14,15,17] Strikingly, a so-far unreported second emission band was observed at around 0.9 eV. At room temperature, a linear dependence of the PL intensity as a function of the excitation fluence was observed for both the 1.9 and 0.9 eV peaks, suggesting a similar recombination mechanism for both emission bands (Figure S1a). At 4.4 K, the high-energy peak shows a sublinear dependence of the PL on the excitation power, which confirms that this emission is dominated by transitions from defects in the band gap as the trap states saturate (Figure S1b).[25] The detection of this low-energy emission is a fingerprint of the trap states deep within the band gap and could explain the poor performance of $Cs_2AgBiBr_6$ solar cells. Although the exact chemical nature of these defects remains to be investigated, DFT calculations have suggested that Ag vacancies and Ag_{Bi} antisites have low formation energies with deep energy levels.[26] A proposed schematic of the relevant recombination processes is shown in Figure 2b.

The diffuse reflectance Kubelka–Munk transformations of the Cu-doped LFDPs are shown in Figure 3a. The crystals with a high copper content show two additional broad absorption bands centered at around 1.7 and 1.2 eV, which is in agreement with the color change of the crystals. It is important to underline that a precise identification of the energy of the lowest-energy peak is difficult in our measurements because of the large influence of environmental absorption at this wavelength. The reduction of the absorption near 0.65 and 0.85 eV is related to water absorption, see the Supporting Information for further details. In traditional doping of semiconductors, shallow energy states close to the band edges form to increase the charge transport at room temperature. In contrast, we observed the formation of deep energy states, which act more as traps than as doping states. As discussed above, the doping mechanism of Cu naturally creates additional Ag^+ vacancy defects. The high absorption ranging from 0.5 to 2 eV shows that the copper doping introduces absorption bands within the band gap that originate from a large number of electronic transitions most likely due to the Cu level and the induced defects (vide infra), although our measurements cannot distinguish which of the two is dominant.[27,28] We highlight that the absorption band at the low energy extends to a much lower energy than reported previously, potentially caused by the higher concentration of Cu in our material.[20]

The PL spectra of the crystals at room temperature—focusing on the visible part of the spectrum—are presented in Figure 3b (see Figure S2 for spectra covering the near-infrared region). On increasing the copper content in the crystal, the 1.9 eV PL peak is severely quenched. In parallel, the 0.9 eV peak, as discussed in Figures 2a and S2, is also quenched. Interestingly, while these peaks are fully quenched, an as yet unreported PL peak centered at around 1.3 eV appears (see also Figures S2 and S3a). The emission at 1.3 eV is expected to originate from the Cu-related energy band. This suggests that the introduction of Cu-related defect levels in the band gap inhibits efficient relaxation to the deep defect levels present in the pristine material. We note that the discrepancy in the peak maximum in Figures 3b and S2 in the energy range around 1.2 eV stems from the difficulty of spectral correction at the limit of the sensitivity of our setups.

To understand the observed optical properties, both steady-state PL and time-resolved PL (TRPL) were measured at 4.4 K and are presented in Figure 3c and d, respectively. All crystals show a single PL band at approximately 1.99 eV. The PL decay lifetimes of this peak are around 40 μs, with faster lifetimes down to 28 μs for increasing the copper concentrations, as shown in Figure S3b. The faster decay for D4 and D5 indicates a pronounced PL quenching effect for high copper concentrations due to an increased defect density that increases the nonradiative recombination. Interestingly, the

https://doi.org/10.1021/acs.jpclett.1c03035
J. Phys. Chem. Lett. 2021, 12, 10444–10449

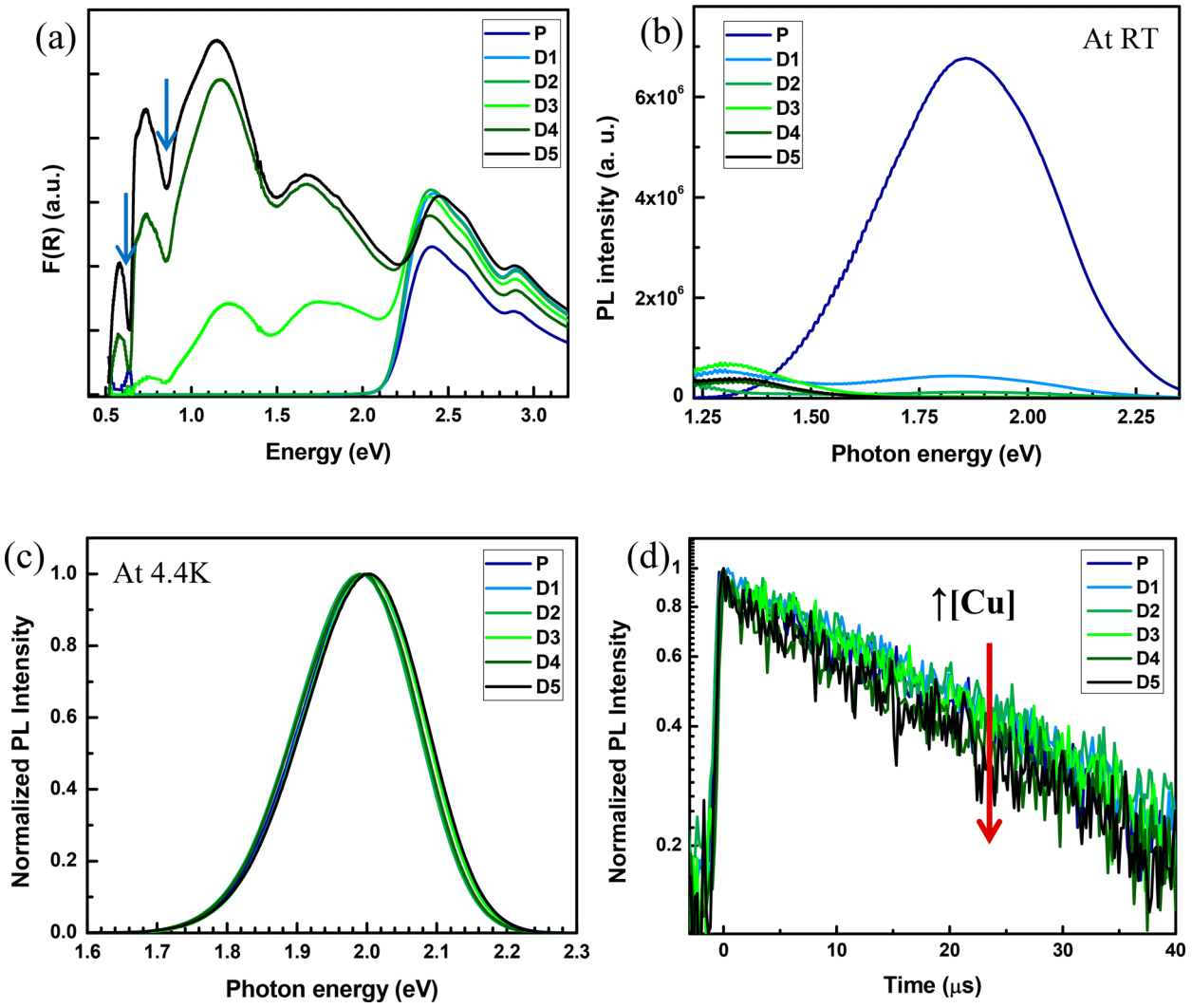

Figure 3. (a) Kubelka−Munk-transformed diffuse reflectance spectra, where the blue arrows indicate the regions affected by water absorption. (b) Photoluminescence spectra at room temperature, (c) normalized steady-state spectra, and (d) time-resolved photoluminescence spectra of P and D1−D5 crystals measured at 4.4 K.

1.3 eV PL band of D1−D5 observed at room temperature, as discussed in Figure 3b, disappears at cryogenic temperatures. To understand this observation, we discuss the two extremes of this set of materials, P and D5, in greater detail.

Figure 4a presents the integrated PL intensity of the 1.9 and 1.3 eV peaks at increasing temperatures, where the lines are a guide to the eye. From 4.4 to 70 K, the PL peak intensities of P and D5 follow a similar trend where they both increase. This trend, termed negative thermal quenching, can be associated either with a lower-energy state that is nonradiative or with the presence of an energy barrier between electronic states. In our case, this could be either a lower-lying defect level or thermal energy being required for the charge carriers to hop to the defect levels.[15] Evidence of the trapping of charge carriers at lower energy states is provided by the fast component of the time-resolved decay of the 1.9 eV peak at low temperatures (Figure S4), which is absent for higher temperatures.[29] Above 70 K, the 1.9 eV peak of the crystals starts to decrease in intensity. For the D5 crystal, the 1.9 eV peak becomes rapidly quenched above 100 K, whereas the 1.3 eV emission band emerges above 120 K and continues to increase in intensity up to 180 K. This negative thermal quenching might be associated with an energy barrier for the charge carriers to relax from a higher energy state to the 1.3 eV state; in other words, thermal energy is used as a means to populate the radiative 1.3 eV state. At higher temperatures, the positive thermal quenching dominates the overall intensity, and the 1.3 eV peak again decreases in intensity together with the 1.9 eV peak. Hence, copper doping in the $Cs_2AgBiBr_6$ structure generates defect levels that are related to two observations: (1) the PL quenching of the 0.9 and 1.9 eV transitions and (2) the transition at 1.3 eV that is thermally activated. In Figure 4b, we propose a possible schematic of the mechanism responsible for the observed PL transitions.

In the plot of PL peak positions against temperature (Figure S5), both pristine and doped crystals present large shifts in the PL peak position between 10 and 40 K that could indicate a phase transition at these low temperatures.[30] To verify this, heat capacity measurements of the crystals were realized and the results show peaks at ∼120 K for both samples that can be attributed to the previously reported cubic-to-tetragonal phase transition of $Cs_2AgBiBr_6$.[29] A small, but noticeable, anomaly around 37 K was detected only for the pristine material (Figure S6). To relate this anomaly with a possible structural

https://doi.org/10.1021/acs.jpclett.1c03035
J. Phys. Chem. Lett. 2021, 12, 10444−10449

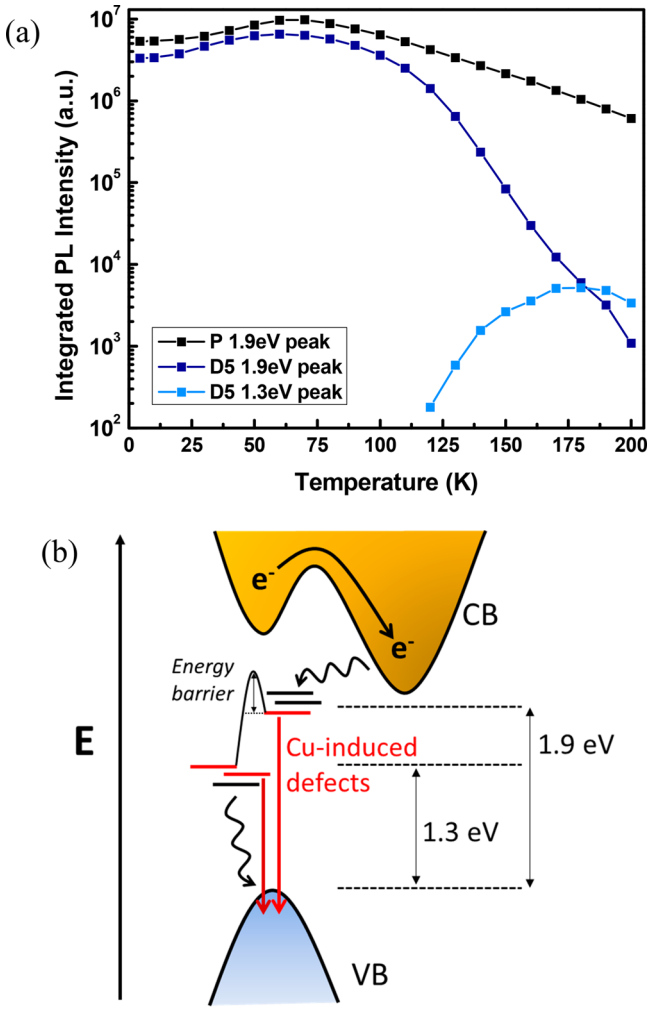

Figure 4. (a) Integrated photoluminescence intensity plotted against temperature for P and D5 crystals and (b) schematic of the radiative recombination pathways associated with the defects in $Cs_2AgBiBr_6$ and the energy levels created by copper doping.

transition, we performed Raman spectroscopy at low temperatures. Additional peaks were observed at 78 and 174 cm^{-1} for the pristine crystal below 50 K and imply a structural transition (Figures S7a, S8a, and S8b). Unexpectedly, the Cu-doped $Cs_2AgBiBr_6$ crystal shows no signature of such a transition in either the the heat capacity data or the Raman data (Figures S7b, S8c, and S8d). This suggests that the disorder introduced by copper inhibits the structural transition. Further discussion on the effect of copper doping in the $Cs_2AgBiBr_6$ structure at low temperatures is presented in the SI.

To conclude, in this study we doped $Cs_2AgBiBr_6$ single crystals with different concentrations of Cu^{2+} and analyzed their fundamental structural and optical properties in detail. The newly reported photoluminescence at of the pristine $Cs_2AgBiBr_6$ 0.9 eV highlights that defects dominate the optical properties of this material. We demonstrate that copper doping shifts the Raman modes without changing the crystal structure. The copper doping introduces additional defect levels that extend the absorption until 0.5 eV and greatly quench the PL, where a so-far unreported emission band at around 1.3 eV appears. This new emission band only lumineses above 120 K, showing that thermal energy is necessary to trigger the copper-related emission. Moreover, Raman and heat capacity data measured until 4.4 K show evidence of a phase transition of $Cs_2AgBiBr_6$ crystals at 37 K that is possibly suppressed by the introduction of copper into the structure. The presented results are important for comprehending the chemistry and physics of double perovskite doping and contribute to the fundamental understanding of this class of materials.

■ ASSOCIATED CONTENT

Supporting Information

The Supporting Information is available free of charge at https://pubs.acs.org/doi/10.1021/acs.jpclett.1c03035.

Additional synthesis and experimental details, inductively coupled plasma results, photoluminescence vs excitation fluence plot, photoluminescence at the near-infrared region spectra, temperature-dependent photoluminescence transients, temperature-dependent photoluminescence peak position, heat capacity curves, and Raman spectra at low temperatures(PDF)

■ AUTHOR INFORMATION

Corresponding Authors

Ana Flavia Nogueira − *Laboratório de Nanotecnologia e Energia Solar, Chemistry Institute, University of Campinas, Campinas 13083-970 São Paulo, Brazil;* orcid.org/0000-0002-0838-7962; Email: anafla@unicamp.br

Maria A. Loi − *Zernike Institute for Advanced Materials, University of Groningen, Groningen 9747 AG, The Netherlands;* orcid.org/0000-0002-7985-7431; Email: m.a.loi@rug.nl

Authors

Bruno I. Ito − *Laboratório de Nanotecnologia e Energia Solar, Chemistry Institute, University of Campinas, Campinas 13083-970 São Paulo, Brazil;* orcid.org/0000-0003-2016-7679

Eelco K. Tekelenburg − *Zernike Institute for Advanced Materials, University of Groningen, Groningen 9747 AG, The Netherlands;* orcid.org/0000-0001-8962-5434

Graeme R. Blake − *Zernike Institute for Advanced Materials, University of Groningen, Groningen 9747 AG, The Netherlands;* orcid.org/0000-0001-9531-7649

Complete contact information is available at: https://pubs.acs.org/10.1021/acs.jpclett.1c03035

Notes

The authors declare no competing financial interest.

■ ACKNOWLEDGMENTS

B.I.I. and E.K.T. contributed equally to this work. B.I.I. and A.F.N. gratefully acknowledge support from FAPESP (the Sao Paulo Research Foundation, Process 2017/11986-5) and the Shell Company as well as the strategic importance of the support given by ANP (Brazil's National Oil, Natural Gas, and Biofuels Agency) through the R&D levy regulation. E.K.T acknowledges the financial support of the Zernike Institute of Advanced Materials. The authors acknowledge technical support from A.F. Kamp, T. Zaharia, J. Baas, D. A. Simoni, and R. Pereira.

REFERENCES

(1) Kojima, A.; Teshima, K.; Shirai, Y.; Miyasaka, T. Organometal Halide Perovskites as Visible-Light Sensitizers for Photovoltaic Cells. *J. Am. Chem. Soc.* **2009**, *131*, 6050−6051.

(2) Zhang, J.; Hodes, G.; Jin, Z.; Liu, S. All-Inorganic $CsPbX_3$ Perovksite Solar Cells: Progress and Prospects. *Angew. Chem., Int. Ed.* **2019**, *58*, 15596−15618.

(3) Jiang, Q.; Zhao, Y.; Zhang, X.; Yang, X.; Chen, Y.; Chu, Z.; Ye, Q.; Li, X.; Yin, Z.; You, J. Surface Passivation of Perovskite Film for Efficient Solar Cells. *Nat. Photonics* **2019**, *13*, 460−466.

(4) National Renewable Energy Laboratory (NREL). Best Research-Cell Efficiencies 2020, https://www.nrel.gov/pv/assets/pdfs/best-research-cell-efficiencies.20200406.pdf.

(5) Jena, A. K.; Kulkarni, A.; Miyasaka, T. Halide Perovskite Photovoltaics: Background, Status, and Future Prospects. *Chem. Rev.* **2019**, *119*, 3036−3103.

(6) Saliba, M.; Correa-Baena, J.; Wolff, C. M.; Stolterfoht, M.; Phung, N.; Albrecht, S.; Neher, D.; Abate, A. How to Make over 20% Efficient Perovskite Solar Cells in Regular (n−i−p) and Inverted (p−i−n) Architectures. *Chem. Mater.* **2018**, *30*, 4193−4201.

(7) Wang, R.; Wang, J.; Tan, S.; Duan, Y.; Wang, Z.; Yang, Y. Opportunities and Challenges of Lead-Free Perovskite Optoelectronic Devices. *Trends in Chemistry* **2019**, *1*, 368−379.

(8) Babayigit, A.; Ethirajan, A.; Muller, M.; Conings, B. Toxicity of Organometal Halide Perovskite Solar Cells. *Nat. Mater.* **2016**, *15*, 247−251.

(9) Schileo, G.; Grancini, G. Lead or No Lead? Availability, Toxicity, Sustainability and Environmental Impact of Lead-Free Perovskite Solar Cells. *J. Mater. Chem. C* **2021**, *9*, 67−76.

(10) Shi, Z.; Guo, J.; Chen, Y.; Li, Q.; Pan, Y.; Zhang, H.; Xia, Y.; Huang, W. Lead-Free Organic−Inorganic Hybrid Perovskites for Photovoltaic Applications: Recent Advances and Perspectives. *Adv. Mater.* **2017**, *29*, 1605005.

(11) Greul, E.; Petrus, M. L.; Binek, A.; Docampo, P.; Bein, T. Highly Stable, Phase Pure $Cs_2AgBiBr_6$ Double Perovskite Thin Films for Optoelectronic Applications. *J. Mater. Chem. A* **2017**, *5*, 19972−19981.

(12) Yang, X.; Chen, Y.; Liu, P.; Xiang, H.; Wang, W.; Ran, R.; Zhou, W.; Shao, Z. Simultaneous Power Conversion Efficiency and Stability Enhancement of $Cs_2AgBiBr_6$ Lead-Free Inorganic Perovskite Solar Cell through Adopting a Multifunctional Dye Interlayer. *Adv. Funct. Mater.* **2020**, *30*, 2001557.

(13) Chu, L.; Ahmad, W.; Liu, W.; Yang, J.; Zhang, R.; Sun, Y.; Yang, J.; Li, X. Lead-Free Halide Double Perovskite Materials: A New Superstar Toward Green and Stable Optoelectronic Applications. *Nano-Micro Lett.* **2019**, *11*, 16.

(14) Hoye, R. L. Z.; Eyre, L.; Wei, F.; Brivio, F.; Sadhanala, A.; Sun, S.; Li, W.; Zhang, K. H. L.; MacManus-Driscoll, J. L.; Bristowe, P. D.; et al. Fundamental Carrier Lifetime Exceeding 1 μs in $Cs_2AgBiBr_6$ Double Perovskite. *Adv. Mater. Interfaces* **2018**, *5*, 1800464.

(15) Wright, A. D.; Buizza, L. R. V.; Savill, K. J.; Longo, G.; Snaith, H. J.; Johnston, M. B.; Herz, L. M. Ultrafast Excited-State Localization in $Cs_2AgBiBr_6$ Double Perovskite. *J. Phys. Chem. Lett.* **2021**, *12*, 3352−3360.

(16) Slavney, A. H.; Hu, T.; Lindenberg, A. M.; Karunadasa, H. I. A Bismuth-Halide Double Perovskite with Long Carrier Recombination Lifetime for Photovoltaic Applications. *J. Am. Chem. Soc.* **2016**, *138*, 2138−2141.

(17) Zelewski, S. J.; Urban, J. M.; Surrente, A.; Maude, D. K.; Kuc, A.; Schade, L.; Johnson, R. D.; Dollmann, M.; Nayak, P. K.; Snaith, H. J.; et al. Revealing the Nature of Photoluminescence Emission in the Metal-Halide Double Perovskite $Cs_2AgBiBr_6$. *J. Mater. Chem. C* **2019**, *7*, 8350−8356.

(18) Palummo, M.; Berrios, E.; Varsano, D.; Giorgi, G. Optical Properties of Lead-Free Double Perovskites by Ab Initio Excited-State Methods. *ACS Energy Lett.* **2020**, *5*, 457−463.

(19) Slavney, A. H.; Leppert, L.; Bartesaghi, D.; Gold-Parker, A.; Toney, M. F.; Savenije, T. J.; Neaton, J. B.; Karunadasa, H. I. Defect-Induced Band-Edge Reconstruction of a Bismuth-Halide Double Perovskite for Visible-Light Absorption. *J. Am. Chem. Soc.* **2017**, *139*, 5015−5018.

(20) Ji, F.; Huang, Y.; Wang, F.; Kobera, L.; Xie, F.; Klarbring, J.; Abbrent, S.; Brus, J.; Yin, C.; Simak, S. I.; et al. Near-Infrared Light-Responsive Cu-Doped $Cs_2AgBiBr_6$. *Adv. Funct. Mater.* **2020**, *30*, 2005521.

(21) McClure, E. T.; Ball, M. R.; Windl, W.; Woodward, P. M. Cs_2AgBiX_6 (X = Br, Cl): New Visible Light Absorbing, Lead-Free Halide Perovskite Semiconductors. *Chem. Mater.* **2016**, *28*, 1348−1354.

(22) Steele, J. A.; Puech, P.; Keshavarz, M.; Yang, R.; Banerjee, S.; Debroye, E.; Kim, C. W.; Yuan, H.; Heo, N. H.; Vanacken, J.; et al. Giant Electron−Phonon Coupling and Deep Conduction Band Resonance in Metal Halide Double Perovskite. *ACS Nano* **2018**, *12*, 8081−8090.

(23) Yu, P. Y.; Cardona, M. Effect of Quantum Confinement on Electrons and Photons in Semiconductors. In *Fundamentals of Semiconductors Physics and Materials Properties*, 2 ed.; Springer-Verlag Berlin Heidelberg GmbH: New York, NY, 1999; p 501.

(24) Filip, M. R.; Hillman, S.; Haghighirad, A. A.; Snaith, H. J.; Giustino, F. Band Gaps of the Lead-Free Halide Double Perovskites $Cs_2BiAgCl_6$ and $Cs_2BiAgBr_6$ from Theory and Experiment. *J. Phys. Chem. Lett.* **2016**, *7*, 2579−2585.

(25) Schmidt, T.; Lischka, K.; Zulehner, W. Excitation-Power Dependence of the Near-Band-Edge Photoluminescence of Semiconductors. *Phys. Rev. B: Condens. Matter Mater. Phys.* **1992**, *45*, 8989−8994.

(26) Xiao, Z.; Meng, W.; Wang, J.; Yan, Y. Thermodynamic Stability and Defect Chemistry of Bismuth-Based Lead-Free Double Perovskites. *ChemSusChem* **2016**, *9*, 2628−2633.

(27) Ji, F.; Klarbring, J.; Wang, F.; Ning, W.; Wang, L.; Yin, C.; Figueroa, J. S. M.; Christensen, C. K.; Etter, M.; Ederth, T.; et al. Lead-Free Halide Double Perovskite $Cs_2AgBiBr_6$ with Decreased Bandgap. *Angew. Chem., Int. Ed.* **2020**, *59*, 15191−15194.

(28) Karmakar, A.; Dodd, M. S.; Agnihotri, S.; Ravera, E.; Michaelis, V. K. Cu(II)-Doped $Cs_2SbAgCl_6$ Double Perovskite: A Lead-Free, Low-Bandgap Material. *Chem. Mater.* **2018**, *30*, 8280−8290.

(29) Schade, L.; Wright, A. D.; Johnson, R. D.; Dollmann, M.; Wenger, B.; Nayak, P. K.; Prabhakaran, D.; Herz, L. M.; Nicholas, R.; Snaith, H. J.; et al. Structural and Optical Properties of $Cs_2AgBiBr_6$ Double Perovskite. *ACS Energy Lett.* **2019**, *4*, 299−305.

(30) Keshavarz, M.; Debroye, E.; Ottesen, M.; Martin, C.; Zhang, H.; Fron, E.; Küchler, R.; Steele, J. A.; Bremholm, M.; Van de Vondel, J.; et al. Tuning the Structural and Optoelectronic Properties of $Cs_2AgBiBr_6$ Double-Perovskite Single Crystals through Alkali-Metal Substitution. *Adv. Mater.* **2020**, *32*, 2001878.

https://doi.org/10.1021/acs.jpclett.1c03035
J. Phys. Chem. Lett. 2021, 12, 10444−10449